Infrared Spectra and Structures of Nickel and Palladium Dinitrosyl Complexes Isolated in Solid Argon

Mohammad Esmaïl Alikhani, Lahouari Krim, and Laurent Manceron*

LADIR/Spectrochimie Moléculaire, UMR 7075 CNRS, Université Pierre et Marie Curie, Boîte 49, 4 Place Jussieu, 75252 Paris, Cedex 05, France

Received: March 27, 2001; In Final Form: June 5, 2001

The infrared spectrum of nickel and palladium dinitrosyls formed by reaction of ground-state Ni or Pd atoms with NO during condensation in solid argon has been reinvestigated, and the energetic, structural, and spectroscopic properties of these compounds have been calculated using density functional theory. The Pd(η^1-NO)$_2$ molecule, already characterized in reactions of laser-ablated Pd, is the only product formed in the reaction between one Pd atom and two nitric oxide molecules. With Ni, in contrast, two different isomeric forms are evidenced, Ni (η^1-NO)$_2$ and Ni (η^2-NO)$_2$, differing by the metal coordination modes and electronic structures. For the M(η^1-NO)$_2$, M = Ni and Pd, species, four additional fundamentals have been measured in the mid- and far-infrared regions for various isotopic species. If the experimental results only show that the complex is centrosymmetrical, the existence of two IR-active vibrations in the far-infrared region and the data for the asymmetrical isotopomers are consistent with a linear structure predicted by DFT calculations. For the Ni(η^2-NO)$_2$ → Ni(η^1-NO)$_2$ conversion, estimates of the transition state energetic and structural properties are consistent with the experimental data. The changes in electronic structure and the reinforcement of the coordination bond when going from mono- to dinitrosyls are discussed in light of the results of a topological analysis of the bonding.

Introduction

The changes in the coordination strength that occur upon successive ligand additions on zerovalent transition metal centers are a central point in inorganic chemistry. Depending how fast the individual binding energy decreases for each addition before complete coordination is reached will govern the thermodynamical stability and to some extent the chemical activity of the complexes.[1] After studying in detail the mononitrosyl of nickel and palladium,[2,3] it is interesting to compare the evolution of structural and electronic properties which can be inferred from the spectral data for the next coordination step, the more stable dinitrosyl species.

In recent studies, among the reaction products of laser-ablated nickel[4] or palladium[5] atoms with NO molecules and along with other MNO^+, MNO, and MNO^-, and M_2NO (M = Ni, Pd) species was provided identification of a $M(NO)_2$ species through the observation of one fundamental and one combination band involving the antisymmetrical NO stretching vibrations. From the spectral data, Zhou, Citra, and Andrews[4,5] concluded that this species contained equivalent nitrosyl groups. These observations were further compared to the predictions of density functional (DF) calculations and found to be in better agreement with the properties predicted for a $^3\Sigma_g^-$ ground state and thus a linear structure. These predictions also contained an intriguing point, which was that the M−N *and* N═O bond distances were calculated slightly *shorter* in the dinitrosyl than in the mononitrosyl compounds for each metal. These predictions had yet to be tested, as the other, low-frequency metal−ligand stretching or bending modes were not detected.

In the course of parallel investigations in this laboratory focusing on the neutral species formed by ground-state Pd and NO reactions, additional information on the dinitrosyl species was obtained. With nickel a specific metastable isomeric form of the dinitrosyl has been evidenced, and for the stable, M(η^1-NO)$_2$, M = Ni and Pd, form, we report here observed or estimated frequencies of the stretching and bending vibrations ν_1, ν_2, ν_3, ν_4, and ν_6 for several isotopic species ($^{14}N^{16}O$, $^{15}N^{16}O$, and $^{14}N^{18}O$ isotopic species for NO) and further DF calculations.

Experimental and Theoretical Procedures

The experimental methods and setup are the same as those described in the preceding paper. To enhance the formation of the larger aggregates, the M + NO species were prepared by co-condensing Pd or Ni vapor with relatively concentrated NO/Ar mixtures (1−4% molar ratios) to have a clear nitric oxide stoichiometric excess, and the population of dinitrosyl complex was also enhanced by annealing the sample from the deposition temperature near 9 K, up to about 35 K. For Ni-containing samples, selective photolyses around 405 nm were conducted using a 200 W HgXe arc lamp focused through a narrow band-pass interference filter.

All calculations have been performed with the Gaussian 98/DFT quantum chemical package,[6] using Becke's three parameters hybrid method[7] and the Lee−Yang−Parr gradient-corrected correlation functional.[8] We have used the 6-311+G(2d) extended basis set of Pople et al.[9] for oxygen and nitrogen. For Ni, the basis set of Schaefer et al.[10] with triple-ζ quality in the valence region (17s10p6d)/[6s3p3d] was chosen. For Pd, the Stuttgart pseudopotential[11] with explicit treatment of the 18 valence electrons was used. The topology of the electron localization function has been examined using the TopMoD package,[12] using the *wfn* file generated by Gaussian 98 with the option *Output═wfn.*

10.1021/jp011142y CCC: $20.00
Published on Web 07/31/2001

TABLE 1: Observed Frequencies[a] for the Various Isotopic Species of $Pd(NO)_2$ Isolated in an Argon Matrix

$Pd(^{14}N^{16}O)_2$	$Pd(^{15}N^{16}O)_2$	$Pd(^{14}N^{16}O)(^{15}NO)$	$Pd(^{14}N^{18}O)_2$	$Pd(^{14}N^{16}O)(^{14}N^{18}O)$	proposed assgnt
433.5 (0.008)	429.5	≈431	424.3	≈432	ν_4 (Σ_u stretch)
n.o.[b]	n.o.	≈419	no	413	ν_2 (Σ_g stretch)
494.5 (0.003)	482.5	488.4	489.6	492.1	ν_6 (Π_u bend)
1730.0	1696.2	1709.6	1691.0	1705.7	ν_3 (Σ_u stretch)
1734.1	1700.4	1713.8	1695.2	1710.0	
1739.0 (1.00)	1705.2	1718.8	1700.0	1714.8	
n.o.	n.o.	1798.3	n.o.	1796.2	ν_1 (Σ_g stretch)
		1803.0		1800.9	
		1808.3		1805.8	
3532.7	3465.2	3503.2	3452.9	3498.9	$\nu_1 + \nu_3$
3523.1	3455	3493.2	3443.1	3488.8	
3513.4 (0.03)	3446.3	3484.5	3434.9	3479.6	

[a] Vibrational frequencies in cm^{-1}; relative IR intensities are in parentheses. [b] Not observed. [c] Frequencies for the main trapping sites are underlined.

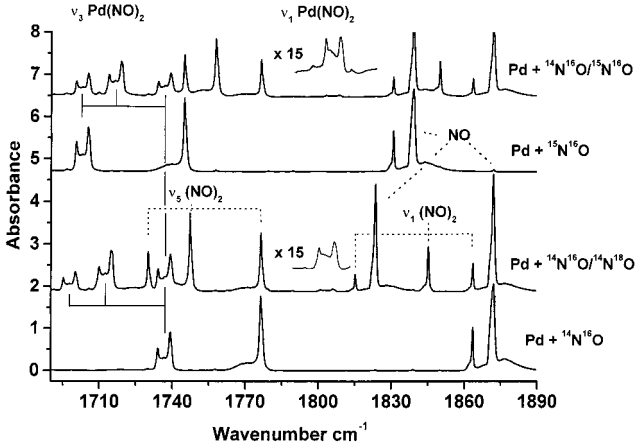

Figure 1. Infrared spectrum in the 1900−1700 cm^{-1} nitrosyl stretching region for various Pd/NO/Ar = 0.2/2/100 isotopic samples.

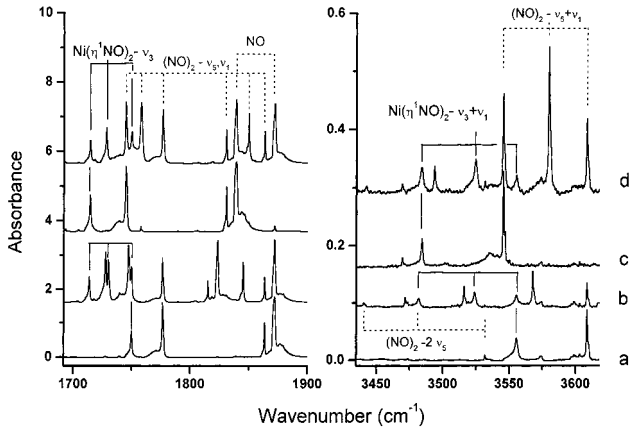

Figure 2. Infrared spectra of nickel η^1-dinitrosyl complexes in the NO stretching fundamental and combination region for various isotopic precursors. From bottom to top: (a) Ni + NO; (b) Ni + ($NO/N^{18}O$ = 1.2); (c) Ni + ^{15}NO; Ni + ($NO/^{14}NO$ = 0.9). The Ni/NO/Ar concentration is approximately 0.5/1/100 in the pure isotopic samples and doubled in the isotopic mixtures. The dotted lines indicate NO and $(NO)_2$ absorptions.

Experimental Results

As described in ref 2, the preceding paper, and in the work of Zhou and Andrews,[4] when Ni or Pd atoms are deposited with relatively concentrated NO/Ar mixtures, strong absorptions are observable near 1750 cm^{-1}. These presented a clear second-order dependence with the nitric oxide concentration and a marked growth after annealing the sample to promote molecular diffusion and were already assigned to the antisymmetrical stretching mode of a dinitrosyl species, $M(\eta^1\text{-}NO)_2$, M = Ni and Pd (see Figures 1 and 2). Also, weaker signals can be easily observed near 3530−3550 cm^{-1}, which were already assigned to the binary combination of symmetrical and antisymmetrical stretching modes of the same species. These absorptions were observed in both works as multiplets, due to the likely occurrence of multiple trapping sites in the argon matrix. Annealing the samples indeed modify slightly the different site populations. Small differences in frequencies appear between this work and that of Zhou or Citra and Andrews, likely due to differences in production modes for the metal vapor production (thermal evaporation with low kinetic energy here vs metal laser ablation processes with high internal and kinetic energy in refs 4 and 5). New absorptions (listed in Tables 1 and 2) were detected in the low-frequency region which correlate with the other bands of this species.

With Ni, another new absorption can be detected in the nitrosyl stretching region at 1343.9 cm^{-1}, at markedly lower frequency. It presents the same concentration dependence as the other bands but belongs to a species different from the other dinitrosyl $Ni(\eta^1\text{-}NO)_2$, as it shows photosensitivity and can be converted into the latter species upon electronic excitation with ≈405 nm light. This species is however energetically stable and can be formed upon matrix annealing and NO molecular diffusion at the expense of the mononitrosyl species.

For all species, the bands appear as triplets in spectra obtained with NO isotopic mixtures ($^{14}N^{16}O/^{15}N^{16}O$ or $^{14}N^{16}O/^{14}N^{18}O$; see Figures 1−6, Tables 1 and 2) and are therefore characteristic of a molecule involving two equivalent NO oscillators, thus Ni- or $Pd(NO)_2$. In addition to the IR-active NO stretching mode, other bands were observed in our work, which are significant to assess the molecular shape and the evolution in coordination bonding for this species.

$Ni(NO)_2$. Figures 5 and 6 present the isotopic effects observed for the low-frequency absorptions near 524 and 624 cm^{-1}. The spectra presented here correspond to samples after annealing up to 30 K, which reduced the number of trapping sites (especially on the 524.4 and 1750.2 cm^{-1} bands). The 524.4 cm^{-1} band is relatively sharp and clearly presents a triplet structure, even with isotopically pure NO precursors. The 18/7/1 relative intensities of the multiplet component matches the natural population of ^{58}Ni, ^{60}Ni, and ^{62}Ni isotopes. The $^{14}N/^{15}N$ effect is smaller than the metal isotope effect, and the ^{14}NO + ^{15}NO mixture clearly splits each metal isotopic component into triplets. The $^{16}O/^{18}O$ effect is larger, and both metal and NO isotopic effects are interleaved. Relative intensity measurements enable assignments of the different isotopic species as labeled on Figure 5. The component corresponding to the isotopically mixed $(N^{16}O)Ni(N^{18}O)$ species is shifted upward

TABLE 2: Observed Frequencies[a] for the Various Isotopic Species of $Ni(NO)_2$ Isolated in an Argon Matrix

$Ni(^{14}N^{16}O)_2$	$Ni(^{15}N^{16}O)_2$	$Ni(^{14}N^{16}O)$ $(^{14}N^{18}O)$	$Ni(^{14}N^{16}O)(^{15}N^{16}O)$	$Ni(^{14}N^{18}O)_2$	proposed assgnt
524.4, 520.1, 516.0 (0.08)	521.8, 517.5, 513.3	519.8, 515.5, 511.7	523.1, 518.7, 514.7	513.4, 509.1, 505.0	$^{58,60,62}Ni(\eta^1\text{-}NO)_2$ ν_4 (Σ_u stretch)
623.9 (0.002)	608.1	621.3	616.1	618.4	$Ni(\eta^1\text{-}NO)_2$ ν_6 (Π_u bend)
1343.9	1320.6	1322.9	1330.6	1308.8	$Ni(\eta^2\text{-}NO)_2$
1750.2 (1)	1714.4	1727.7	1728.5	1713.7	$Ni(\eta^1\text{-}NO)_2$ ν_3 (Σ_u stretch)
3555.4 (0.02)	3483.9	3523.8	3524.8	3481.7	$Ni(\eta^1\text{-}NO)_2$ $\nu_1 + \nu_3$

[a] Vibrational frequencies in cm^{-1}; relative IR intensities are in parentheses.

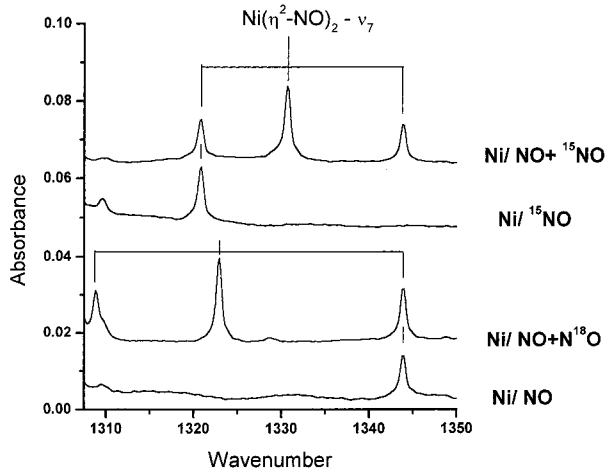

Figure 3. Infrared spectra of the nickel η^2-dinitrosyl in the NO stretching mode region for various isotopic precursors. The experimental conditions are the same as in Figure 2.

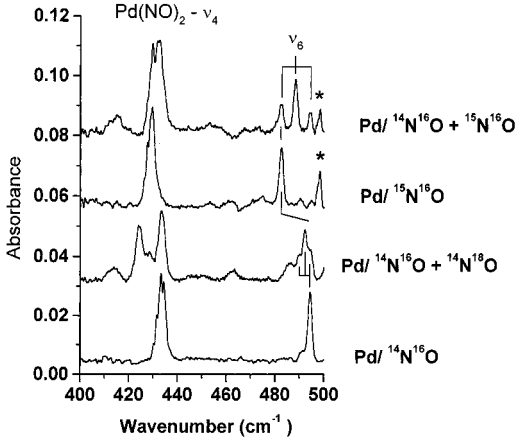

Figure 4. Infrared spectrum in the ν_2, ν_4, and ν_6 regions of $Pd(NO)_2$: (a) $Pd/^{14}N^{16}O/Ar = 0.2/2/100$; (b) same with $^{14}N^{16}O/^{14}N^{18}O = 0.6/0.4$; (c) same with $^{15}N^{16}O$; (d) same with $^{14}N^{16}O + {}^{15}N^{16}O = 0.55/0.45$. The asterisk indicates a ^{15}NO-dimer absorption.

with respect to the average of the isotopically symmetrical components. This indicates that, for the isotopically mixed species, another mode of same symmetry occurs <100 wavenumbers below.

The weaker 623.9 cm^{-1} fundamental presents respectively large and small $^{14}N/^{15}N$ and $^{16}O/^{18}O$ effects which are drastically different from those observed for ν_2 of NiNO present in the same spectral region (principally a Ni−N stretching mode).

$Pd(NO)_2$. First, absorptions at 494.5 and 433.1 cm^{-1} where observed in the low-frequency region, which presented the same concentration and annealing dependence as the known $Pd(NO)_2$ bands. While the 494.5 cm^{-1} band presents a straightforward triplet structure (Figure 4), the 433.5 cm^{-1} band presents an overlapping pattern which deserves special comments. The $^{14}N^{16}O/^{15}N^{16}O$ effect is small with respect to the bandwidth, and the corresponding mixture presents only an unresolved

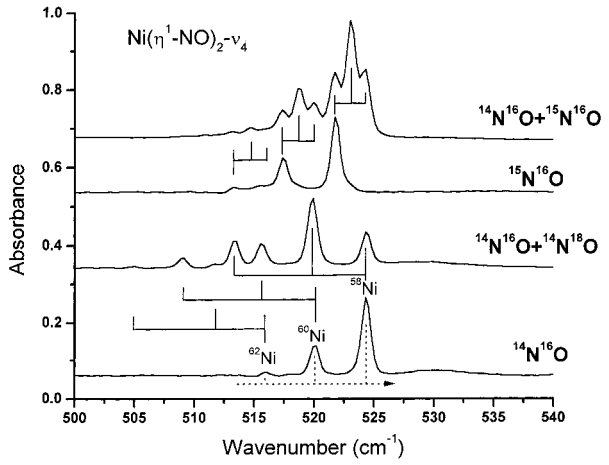

Figure 5. Infrared spectra of nickel η^1-dinitrosyl in the low-frequency stretching region for various isotopic precursors after annealing to about 35 K. The Ni/NO/Ar concentration is approximately 0.5/1/100 in the pure isotopic samples and doubled in the isotopic mixtures. The dotted lines indicate the natural Ni isotopic distribution.

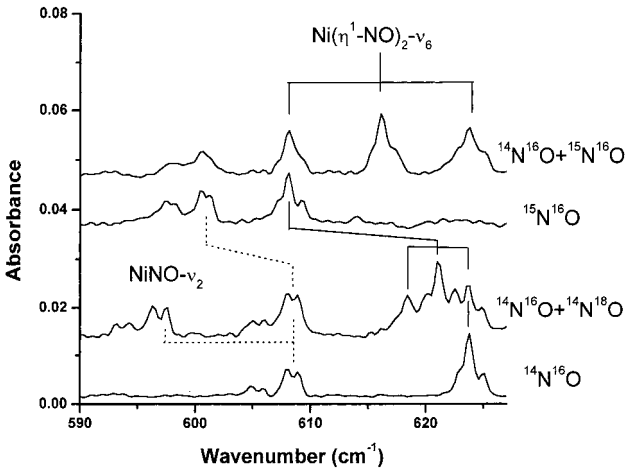

Figure 6. Infrared spectra of nickel η^1-dinitrosyl in the bending mode region for various isotopic precursors after annealing to about 35 K The Ni/NO/Ar concentration is approximately 0.5/1/100 in the pure isotopic samples and doubled in the isotopic mixtures. The dotted lines indicate the Ni−NO ν_2 absorptions present in the same region.

multiplet. Unlike the other band, the $^{14}N^{16}O/^{14}N^{18}O$ effect is larger and, in the $^{14}N^{16}O + {}^{14}N^{18}O$ mixture, the central component due to the $Pd(^{14}N^{16}O)(^{14}N^{18}O)$ species is not observed near the average of the isotopically pure $Pd(^{14}N^{16}O)_2$ or $Pd(^{14}N^{18}O)_2$ species but strongly shifted and overlapping the $Pd(^{14}N^{16}O)_2$ one. Meanwhile an additional, weaker signal appears on the low-frequency side of the $Pd(^{14}N^{18}O)_2$ species, near 415 cm^{-1}.

New supplementary signals are also observed near 1800 cm^{-1} *specifically* in the $^{14}N^{16}O + {}^{15}N^{16}O$ or $^{14}N^{16}O + {}^{14}N^{18}O$ isotopic mixture experiments, thus only for the asymmetric $Pd(^{14}N^{16}O)(^{14}N^{18}O)$ or $Pd(^{14}N^{16}O)(^{15}N^{16}O)$ isotopomers. The present vibrational data are in agreement with those by Citra and

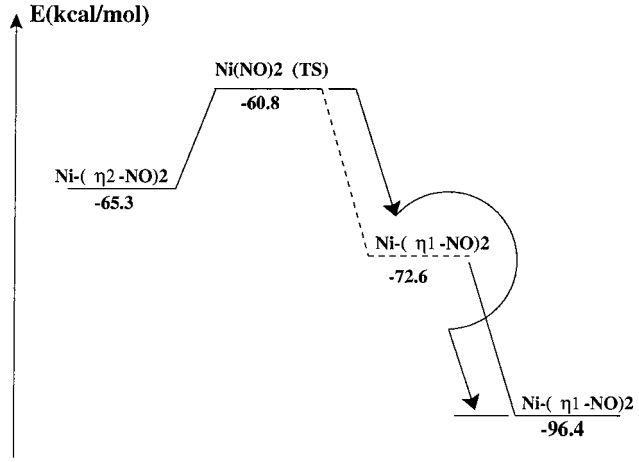

Figure 7. Schematic representation of the isomerization pathway in the $Ni(NO)_2$ system. For the $\eta^2\ ^1A_1$ state $R_{NiN} = 1.782$ Å, $R_{NO} = 1.216$ Å, $\alpha_{NiNO} = 80°$, $\alpha_{NNiN} = 130°$. For the TS (C_2 symmetry) $R_{NiN} = 1.682$ Å, $R_{NO} = 1.166$, $\alpha_{NiNO} = 143°$, $\alpha_{NNiN} = 124°$, dihedral angle (NNiNO) = 112°.

Andrews for the strongly absorbing antisymmetric stretching mode ν_4 and its combination with the totally symmetric one, $\nu_1 + \nu_3$. The present observation of the ν_1 mode for the asymmetric $Pd(^{14}N^{16}O)(^{14}N^{18}O)$ or $Pd(^{14}N^{16}O)(^{15}N^{16}O)$ isotopic species enables an estimate of the anharmonicity corrections for these isotopomers ($X_{13} \approx -24$ cm^{-1}) and thus placing ν_1 around 1820 cm^{-1}, in a region totally void of related absorptions. The ν_1 mode was not observed for the isotopically symmetrical species, which means that, given the signal-to-noise ratio in our experiments, it must be at least 500 times weaker than ν_3 and 15 times less intense than the $\nu_1 + \nu_3$ binary level. This therefore constitutes strong evidence that the molecule is centrosymmetrical.

Theoretical Results and Discussion

$Ni(NO)_2$. For the nickel dinitrosyl system, after the singlet and triplet potential energy surfaces were thoroughly scanned, two different structures corresponding to two different electronic spin multiplicities were calculated to be stable. Let us first recall that, for the mononitrosyl system, two different isomeric forms could be experimentally and theoretically characterized, a Ni(η^1-NO) end-on coordinated species with a bent structure and Ni(η^2-NO) cyclic species with a larger charge transfer.[2] Addition of a second NO molecule to the mononitrosyl results into two possible minima on the singlet surface. One minimum corresponds to a doubly bridging form with $^1A_1$ ground state and a structure in which the two NO ligands are close to parallel (Figure 7) and has a + 65 kcal/mol binding energy with respect to the separate fragments (uncorrected for ZPE effects). Exploring the potential surface by varying the bond angles, for instance, leads to another metastable form with very open N−Ni−N and Ni−N═O bond angle, thus tending toward linearity. This form is very close to the only minimum found on the triplet potential energy surface, the linear $^3\Sigma_g^-$ state predicted by Zhou and Andrews[2] and calculated at this level 96.4 kcal/mol below the isolated fragments. In the solid matrix, energy relaxation willl induce spin conversion and hopping on the more stable triplet potential surface (Figure 7). Tables 3 and 4 present the electronic, geometrical, and vibrational properties predicted for both the $^1A_1$ and the $^3\Sigma_g^-$ states. The strongest IR fundamental frequency predicted for the metastable $^1A_1$ state is in reasonable qualitative agreement with the band observed (1471 cm^{-1} for the ω_7 NO antisymmetric stretching mode compared to 1343.9 cm^{-1}, experimentally) given the usual deviation due to methods and neglect of anharmonicity. The properties calculated for the $^3\Sigma_g^-$ are in agreement with the experimental data for the observed stretching vibrations. The NO stretching vibrations ν_1 and ν_3 are predicted here at 1867 and 1796 cm^{-1}, in reasonable agreement with the observed values (1830 ± 5 and 1750 cm^{-1}, respectively). More interesting are the predicted positions of the ν_2 and ν_4 low-frequency stretching vibrations at 451 and 569 cm^{-1}. The latter is observed at 524 cm^{-1}, and the position of the former can be estimated to be 465 ± 30 cm^{-1}, from a semiempirical fit of the isotopic data using an harmonic force field and a linear geometry. The only notable discrepancy concerns the position of the IR-active bending mode (ν_6 of Π_u symmetry). This frequency is calculated at about 407 cm^{-1} with a vanishing IR intensity, when it is observed at about 624 cm^{-1}

TABLE 3: Calculated Energetic and Vibrational Properties[a] of $Ni(NO)_2$ in the $^1A_1$ and $^3\Sigma_g$ States[b]

params	$Ni(\eta^2\text{-}NO)_2$	$Ni(\eta^1\text{-}NO)_2$	
$D_e(1)$[c] (kcal/mol)	65.3	96.4	
$D_e(2)$[d]	40.9	59.7	
μ (D)	1.04	0	
A_1 sym ($^1A_1$ state)			Σ_g sym ($^3\Sigma_g$ state)
ω_1	1552 (39)	1883 (0)	ω_1
ω_2	693 (1)	456 (0)	ω_2
ω_3	393 (2)		
ω_4	156 (3)		Σ_u sym
A_2 sym		1820 (1598)	ω_3
ω_5	262 (0)	559 (126)	ω_4
B_1 sym			
ω_6	134 (0)		Π_g sym
B_2 sym		267 (0)	ω_5
ω_7	1471 (878)		
ω_8	610 (2)		Π_u sym
ω_9	429 (17)	407 (1)	ω_6
		46 (4)	ω_7
F_{NO} (mdyn/Å)	10.3	13.6	
F_{NiN}	3.2	3.5	

[a] Vibrational harmonic frequencies in cm^{-1}; IR intensities in km/mol. [b] Calculated data for free NO: r = 1.147 Å, ω = 1956 cm^{-1}; F_{NO} = 16.8 mdyn/Å. [c] $D_e(1) = (E_{Ni}(^3D) + 2E_{NO}) - E_{Ni(NO)_2}$. [d] $D_e(2) = (E_{NiNO} + E_{NO}) - E_{Ni(NO)_2}$.

TABLE 4: Comparison of Calculated Energetic and Vibrational Properties[a] of $Pd(NO)_2$ in the $^3\Sigma_g$ State[b] with the Measured IR Frequencies for $Pd(NO)_2$ Isolated in Solid Argon

params for $Pd(\eta^1\text{-}NO)_2$	calcd	exptl	assgnt
$D_e(1)$[c] (kcal/mol)	63.1		
$D_e(2)$[d]	32.9		
μ (D)	0		
Σ_g sym ($^3\Sigma_g$ state)			
ω_1	1892 (0)	1819 ± 5[d]	ν_1
ω_2	426 (0)	430 ± 5[e]	ν_2
Σ_u sym			
ω_3	1816 (2540)	1739	ν_3
ω_4	432 (75)	433	ν_4
Π_g sym			
ω_5	215 (0)		ν_5
Π_u sym			
ω_6	352 (0.5)	494	ν_6
ω_7	41 (1)		ν_7
F_{NO} (mdyn/Å)	14.1		
F_{PdN}	2.9		

[a] Vibrational frequencies in cm^{-1}; IR intensities in km/mol. [b] R_{PdN} = 1.854 Å, R_{NO} = 1.761 Å. $D_e(1) = (E_{Pd(^1S)} + 2E_{NO}) - E_{Pd(NO)_2}$. [c] $D_e(2) = (E_{PdNO} + E_{NO}) - E_{Pd(NO)_2}$. [d] Estimated positions from Pd(NO)(N*O) data and $\nu_1 + \nu_3$. [e] Estimated positions from Pd(NO)(N*O) data and harmonic potential semiempirical calculations.

TABLE 5: Topological ELF Population Analysis (in e)

compds	V(O)[a]	V(N)[a]	V(N, O)[b]	V((N,M)[b]/M[c])	V((O,M)[b]/M[c])	V(M)[a]	C(M)[d]
NO	4.78	3.80	2.17				
Ni(η^1-NO)	5.26	2.94	1.71	1.52/0.66		0.36	26.98
Ni(η^2-NO)	2.95	2.18	1.54	2.3/0.16	2.54/0.09	0.63	27.1
Pd(η^1-NO)	5.15	2.38	1.84	1.78/0.36			45.7
Ni(η^1-NO)$_2$ ($^3\Sigma$)	5.35		1.77	4.64/0.8			26.4
Ni(η^2-NO)$_2$ ($^1A_1$)	3.07	2.41	1.71	2.00/0.24	2.32/0.07		26.4
Pd(η^1-NO)$_2$ ($^3\Sigma$)	5.12		1.89	4.31/0.5			45.00

[a] Monosynaptic basin. [b] Disynaptic basin. [c] M = Ni and Pd metal atom contribution. [d] Core basin.

with about one-sixth of the intensity of the Σ_u symmetry stretching.

As found by Zhou and Andrews,[4] *both* the NO and NiN bond distances are calculated to shorten slightly when going from $^2A'$ NiNO to $^3\Sigma_g^-$ Ni(NO)$_2$. This is also reflected in the slight increase in the NO and NiN harmonic potential constants, but note that the B3LYP results underestimate slightly the metal−ligand vibrations in $^2A'$ NiNO and thus likely the coordination strength for this species. The force constants calculated semiempirically are less different, 4.2 ± 0.4 and 3.6 ± 0.4 mdyn/Å, respectively.

The calculated binding energy per ligand is about +36 kcal/mol for the first and +60 for the second. This difference is in part due to the cost of the triplet−singlet promotion (as the metal electronic configuration in the complexes correlates to the latter) and in part to the change in bonding made possible by the linear structure.

To help understand the formation and stabilization of the Ni(η^2-NO)$_2$ metastable state, we have explored some aspects of the NiNO + NO → Ni(η^2-NO)$_2$ (1) and Ni(η^2-NO)$_2$ → Ni(η^1-NO)$_2$ (2) potential surfaces. First reaction 1 is only energetically feasible when starting from the Ni(η^2-NO) $^2A''$ state. Former studies had shown that the energy difference between the $^2A'$ and $^2A''$ forms was small enough, and the conversion barrier large enough, that both forms could be stabilized in solid argon at low temperature. The approach of a second, $^2\Pi$ NO ligand results in a continuous stabilization on the singlet surface until the Ni(η^2-NO)$_2$ $^1A_1$ state is reached. Note that the binding energy per ligand increases from about 24 to 41 kcal/mol for the first and second ligands, respectively. For reaction 2, the transition state optimized structure and energies are presented in Figure 7. The most favorable isomerization pathway thus involves concerted opening of both Ni−N═O bond angles and twisting of the dihedral angle between the NO groups. Even then it amounts to an estimated 4.5 kcal/mol, which is large enough to warrant stabilization of the metastable form at low temperature.

Pd(NO)$_2$. The molecular shape of the Pd(NO)$_2$ species has been discussed on the basis of density functional calculations which predicted a $^3\Sigma_g$ ground state at the BP91- and B3LYP/LanL2DZ/6-311+G(d) levels of calculation.[5] Other states ($^1A_1$ and ^5B_g) with nonlinear geometries were calculated some 12 and 52 kcal/mol higher in energy. Our calculations with extended basis set confirm these results. The binding energy calculated here amounts to about 63 kcal/mol, a little more than twice the mononytrosyl binding energy (30 kcal/mol). As for the Ni(NO)$_2$ species, the reproduction of the observable data is good for the vibrational fundamental involving stretching coordinates (±2.5%) and deviates by a large factor for the bending vibration (−28%). This kind of situation has been encountered before[13] in the case of strongly coordinated transition metal molecules, but it is yet too early to know whether we are facing a rather specific matrix effect shifting the bending modes of these large linear molecules or a methodological problem affecting this aspect of the reproduction of their vibrational properties. Note that this peculiarity is not observed for the mononitrosyls[2] or oxonitride[14] molecules or the less strongly bound carbonyl systems.[15,16]

In comparison to PdNO, the NO bond distance is calculated slightly shorter, which is confirmed by the slight increase of the bond force constant. The Pd−N bond distance is also calculated to shorten slightly (1.854 vs 1.904 Å). The theoretical Pd−N force constant is calculated to increase in parallel from 2.1 to 2.9 mdyn/Å, but that for PdNO seems obviously underestimated. Semiempirical adjustment procedures yield identical values (3.1± 0.3 mdyn/Å) for both molecules, which is not completely inconsistent, given the error bars. Anyway the change in electronic structure upon addition of the second nitrosyl can lead to a situation in which the ligand is *less* perturbed but the metal−ligand interaction *equivalent or stronger*. This situation can be compared to that observed and calculated by Zhou and Andrews for Cu(NO)$_{1,2}$. In this system as well, addition of a second ligand has a cooperative effect leading to reinforcement of the metal−nitrosyl bonding.

Topological Analysis and Bonding in Dinitrosyls. As for the metal−mononitrosyl compounds, the bonding between the metal atom and nitrosyl units in the case of metal−dinitrosyl has been studied in terms of σ donation/π back-donation using the natural bonding orbital (NBO) method.[17] In the linear triplet state of M(NO)$_2$ (M = Ni or Pd), two hybrid orbitals (σ and σ^*) arise from hybridization between the d_{z^2} and s atomic orbitals allowing NO 5σ donation to the metal σ^* antibonding orbital. The π back-donation occurs from interaction between the two filled metal π orbitals (d_{xz} and d_{yz}) and the semifilled NO π^* antibonding orbital. It should be noted that the NO π^* antibonding orbital is found in the *xz*-plane for the first NO and in the *yz*-plane for the second NO, thus resulting in a triplet ground state.

To provide a quantitative description of the metal−ligand bonding we have studied the systems using the electron localization function (ELF)[18] and the theory of atoms in molecules (AIM).[19] The topological electronic populations are listed in Table 5. One can note that for both metals and both isomeric forms the metal participation in the metal−ligand disynaptic basin increases going from the mononitrosyl to the dinitrosyl compound, which should be paralleled to the increase in binding energies. Also it is interesting to note that the total metal contribution in the metal−ligand disynaptic basin decreases from Ni to Pd reflecting the binding energy variation.

There is no metal monosynaptic basin for both metal−dinitrosyl systems, indicating the participation of the latter basin in the metal−ligand bonding, concomitant with the participation of the metal core basin in the bonding (the decrease of the C(M) population from the mononitrosyl complex to the dinitrosyl complex). This contribution is always smaller than one electron because of the nitrosyl radical character. Finally, the bonding in the nickel and palladium dinitrosyl compounds could be

considered as a metal contribution in the metal−ligand disynaptic basin which is essentially localized on the nitrogen atoms.

References and Notes

(1) Bursten, B.; Green, M. R. *Progress in Inorganic Chemistry*; Wiley: New York, 1998; Vol. 36, p 313.

(2) Krim, L.; Manceron, L.; Alikhani, M. E. *J. Phys. Chem. A* **1999**, *103*, 2598.

(3) Krim, L.; Alikhani, M. E..; Manceron, L. *J. Phys. Chem. A* **2001**, *105*, 7812.

(4) Zhou, M.; Andrews, L. *J. Phys. Chem. A* **2000**, *104*, 3915.

(5) Citra, A.; Andrews, L. *J. Phys. Chem. A* **2000**, *104*, 8160.

(6) Frisch, M. J.; Trucks, G. W.; Schlegel, H. B.; Gill, P. M. W.; Johnson, B. G.; Robb, M. A.; Cheeseman, J. R.; Keith, T.; Petersson, G. A.; Montgomery, J. A.; Raghavachari, K.; Al-laham, M. A.; Zakrzewski, V. G.; Ortiz, J. V.; Foresman, J. B.; Cioslowski, J.; Stefanov, B. B.; Nanayakkara, A.; Challacombe, M.; Peng, C. Y.; Ayala, P. Y.; Chen, W.; Wong, M. W.; Andres, J. L.; Replogle, E. S.; Gomperts, R.; Martin, R. L.; Fox, D. J.; Binkley, J. S.; Defrees, D. J.; Baker, J.; Stewart, J. P.; Head-Gordon, M.; Gonzalez, C.; Pople J. A. *Gaussian 98 (Revision A.7)*; Gaussian, Inc.: Pittsburgh, PA, 1998.

(7) Becke, A. D. *J. Chem. Phys.* **1993**, *98*, 5648.

(8) Lee, C.; Yang, W.; Parr, R. G. *Phys. Rev. B* **1988**, *37*, 785.

(9) Frisch, M. J.; Pople, J. A.; Binkley, J. S. *J. Chem. Phys.* **1984**, *80*, 3265.

(10) Schaefer, A.; Huber. C.; Ahlrichs, R. *J. Chem. Phys.* **1994**, *100*, 5829.

(11) Andrae, D.; Haeussermann, U.; Dolg, M.; Stoll, H.; Preuss, H. *Theor. Chim. Acta* **1990**, *77*, 123.

(12) Noury, S.; Krokodis, X.; Ahlrichs, R.; Silvi, B. Available from http://www.lct.jussieu.fr/silvi.

(13) Manceron, L.; Alikhani, M. E.; Tremblay, B. *J. Phys. Chem. A* **2000**, *104*, 3750.

(14) Krim, L.; Prot, C.; Alikhani, M. E.; Manceron, L. *Chem. Phys.* **2000**, *254*, 267.

(15) Manceron, L.; Alikhani, M. E. *Chem. Phys.* **1999**, *244*, 215.

(16) Tremblay, B.; Manceron, L. *Chem. Phys.* **1999**, *250*, 187.

(17) Zhou, M. F.; Andrews, L. *J. Phys. Chem. A* **2000**, *104*, 2618.

(18) Reed, A. E.; Curtiss, L. A.; Weinhold, F. *Chem. Rev.* **1988**, *80*, 899.

(19) Silvi, B.; Savin, A. *Nature* **1994**, *371*, 683.

(20) Bader, R. F. W. *Atom in Molecules: A Quantum Theory*; Oxford University Press: Oxford, U.K., 1994.